Cell Reports, Volume *22*

Supplemental Information

Nuclear Organization in the Spinal Cord Depends on Motor Neuron Lamination Orchestrated by Catenin and Afadin Function

Carola Dewitz, Sofia Pimpinella, Patrick Hackel, Altuna Akalin, Thomas M. Jessell, and Niccolò Zampieri

Supplemental experimental procedures

Mouse strains

Afadin^{fl} (Beaudoin III et al., 2012), *β-cat*^{fl} (Brault et al., 2001), *γ-cat*^{fl} (Demireva et al., 2011) *N-cadherin*^{fl} (Kostetskii et al., 2005), *rosa-lsl-tdTomato* (Ai14, Madisen et al., 2010) and *olig2::Cre* (Dessaud et al., 2007) mouse lines have been previously described. *Afadin*$^{-}$ mouse line was obtained by crossing the *Afadin*^{fl} line with *Protamine::Cre* line to achieve germline deletion (O'Gorman et al., 1997). All experimental procedures were performed according to the policies of the Max-Delbrück-Center for Molecular Medicine.

Immunohistochemistry

Immunohistochemistry analysis was performed using the following primary antibodies: rabbit anti-afadin (Abcam AB11337), mouse anti-Lhx3 (DSHB Hybridoma Product 67.4E12), rabbit anti-nectin 4 (Abcam ab155692), rat anti-nectin 1 (MBL D146-3), rat anti-nectin 2 (MBL D083-3), rat anti-nectin 3 (MBL D084-3), sheep anti-nNOS (Merck Millipore AB1529). Other antibodies were described in: Agalliu et al., 2009; Dasen et al., 2008; De Marco Garcia and Jessell, 2008. Guinea pig anti-afadin was generated using the following synthetic peptide: CRKLTELENELNTK.

Motor neuron subtypes identification

Motor neuron divisional subtypes were identified by the expression of homeobox transcription factors Isl1/2 (LMCm) and Hb9 (LMCl; Sockanathan and Jessell, 1998). Motor pools occupying different medio-lateral and dorso-ventral positions at lumbar spinal levels were identified by expression of homeobox and ETS transcription factors

(De Marco Garcia and Jessell, 2008). The adductor/gracilis (A/G) pool was identified by expression of Er81 and Nkx6.1; the rectus femoris/tensor fasciae latae (R/T) complex was identified by expression of Nkx6.2; the hamstrings (H) complex was identified by expression of Nkx6.1 and the vasti (V) motor pool was identified by expression of Er81.

Statistical analysis

Contour and density plots were generated using "ggplot2" package by estimating the Gaussian kernel density for the distribution of neuron positions. Contour plots were calculated from 2D density estimates of neuron positions using a bivariate normal kernel on a 100x100 grid. These calculations rely on the "kde2D" function in the MASS library. We used correlation heat maps to compare the 2D spatial distribution of neurons across experiments. In order to produce the heat maps, we first computed 2D density estimates of positions on a 100x100 grid. The similarity between pairs of experiments was measured by the Pearson correlation coefficient of the 2D density estimates on the 100x100 grid. The heat map was then ordered using hierarchical clustering with complete linkage method and the distance metric as $1-r$, where r is the Pearson correlation coefficient. The package "corrplot" was used for plotting and ordering the heat map.

Supplemental references

Agalliu, D., Takada, S., Agalliu, I., McMahon, A.P., and Jessell, T.M. (2009). Motor Neurons with Axial Muscle Projections Specified by Wnt4/5 Signaling. Neuron 61, 708–720.

Brault, V., Moore, R., Kutsch, S., Ishibashi, M., Rowitch, D.H., McMahon, a P., Sommer, L., Boussadia, O., and Kemler, R. (2001). Inactivation of the beta-catenin gene by Wnt1-Cre-mediated deletion results in dramatic brain malformation and failure of craniofacial development. Development 128, 1253–1264.

Kostetskii I., Li J., Xiong Y., Zhou R., Ferrari V.A., Patel V. V., Molkentin J.D., and Radice G.L. (2005). Induced deletion of the N-cadherin gene in the heart leads to dissolution of the intercalated disc structure. Circ. Res. *96*, 346–354.

Madisen L., Zwingman T.A., Sunkin S.M., Oh S.W., Zariwala H.A., Gu H., Ng L.L., Palmiter R.D., Hawrylycz M.J., Jones A.R., Lein E.S., Zeng H. (2010). A robust and high-throughput Cre reporting and characterization system for the whole mouse brain. Nat. Neurosci. *13*(1):133-40.

O'Gorman S., Dagenais N.A., Qian M., Marchuk Y. (1997). Protamine-Cre recombinase transgenes efficiently recombine target sequences in the male germ line of mice, but not in embryonic stem cells. Proc. Natl. Acad. Sci. USA *94*(26): 14602-7.

Table S1. Genotypes, number of embryos, and number of sections per embryo analyzed for three-dimensional positional analysis, related to Experimental Procedures

Experiment	MN Subtype	Genotype	# of Embryos	# of Sections/Embryo
"control"	Divisions	*afadin fl/+*	3	33 27 30
"control"	Pools	*afadin fl/+*	3	31 29 30
"afadin$^{\Delta MN}$"	Divisions	*afadin fl/-;* *olig2::Cre+/-*	3	27 26 24
"afadin$^{\Delta MN}$"	Pools	*afadin fl/-;* *olig2::Cre+/-*	3	28 32 27
"N$^{\Delta MN}$"	Divisions	*N-cadherin fl/-;* *olig2::Cre +/-*	3	20 30 31
"N$^{\Delta MN}$"	Pools	*N-cadherin fl/-;* *olig2::Cre +/-*	3	30 26 31
"βγ$^{\Delta MN}$"	Divisions	*β-catenin fl/fl;* *γ-catenin fl/-;* *olig2::Cre+/-*	3	31 32 30
"βγ$^{\Delta MN}$"	Pools	*β-catenin fl/fl;* *γ-catenin fl/-;* *olig2::Cre+/-*	3	25 28 28

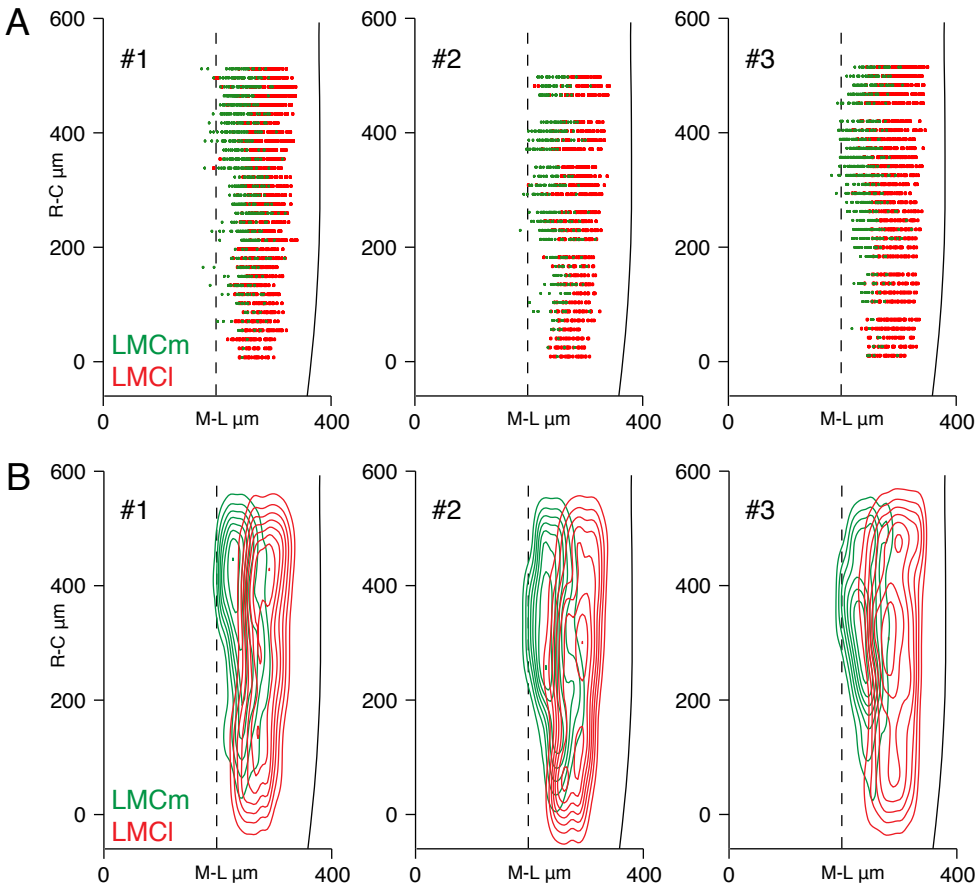

Figure S1. Divisional rostro-caudal position analysis in e13.5 control embryos, related to Figure 1.
(A) Longitudinal digital reconstruction of LMCm (green) and LMCl (red) neuronal positions for e13.5 control embryos (n= 3).
(B) Longitudinal contour density analyses of LMCm (green) and LMCl (red) neurons for e13.5 control embryos (n= 3).

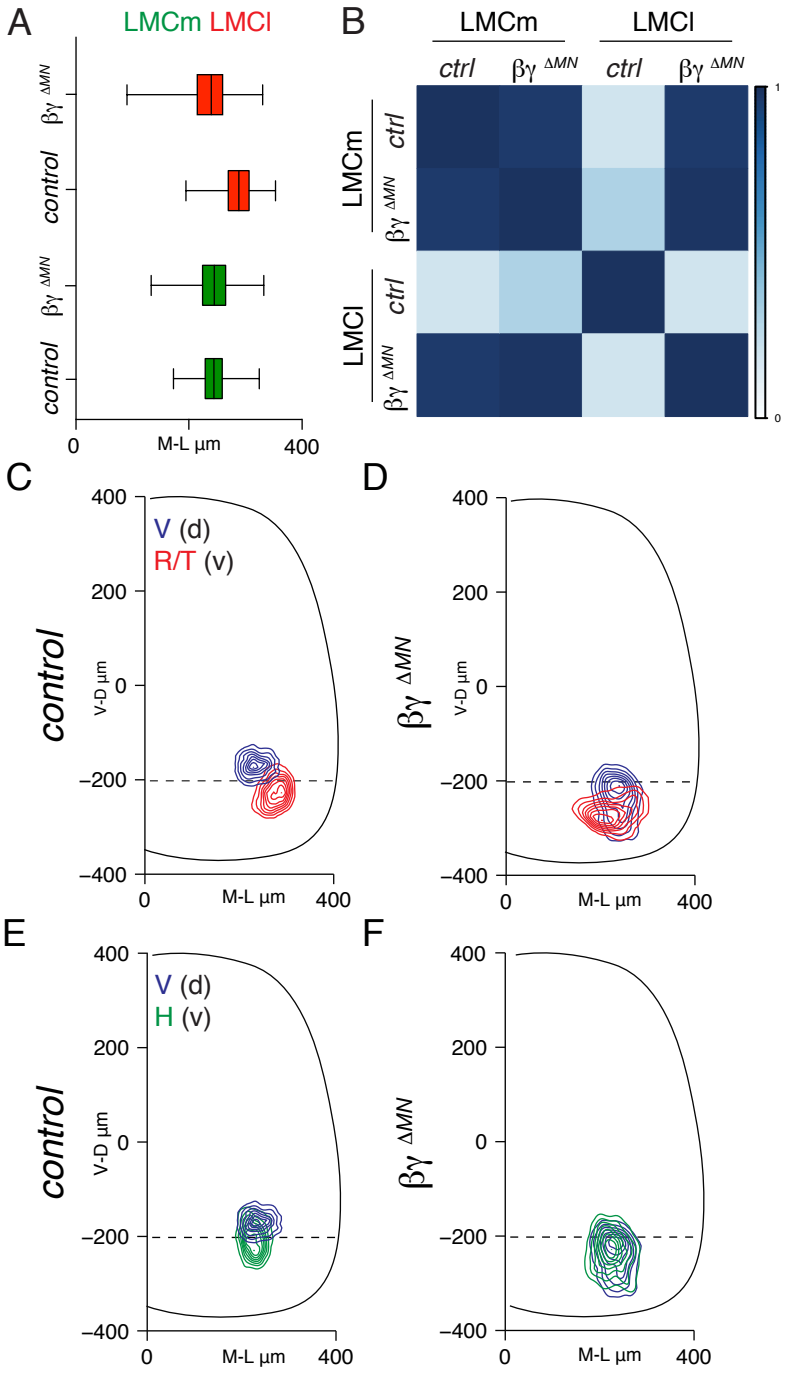

Figure S2. Divisional and pool positional analysis in e13.5 β- and γ- catenin mutant embryos, related to Figure 2 and 3.

(A) Box-plots showing distributions of LMCm (green) and LMCl (red) neurons in *control* and $\beta\gamma^{\Delta MN}$ embryos.

(B) Correlation analysis of LMC positional coordinates on medio-lateral axis in *control* and $\beta\gamma^{\Delta MN}$ embryos. Scale bar indicates correlation values.

(C and D) Transverse contour density analyses of V (blue; dorsal) and R/T (red; ventral) motor pools in *control* and $\beta\gamma^{\Delta MN}$ embryos.

(E and F) Transverse contour density analyses of V (blue; dorsal) and H (green; ventral) motor pools in *control* and $\beta\gamma^{\Delta MN}$ embryos.

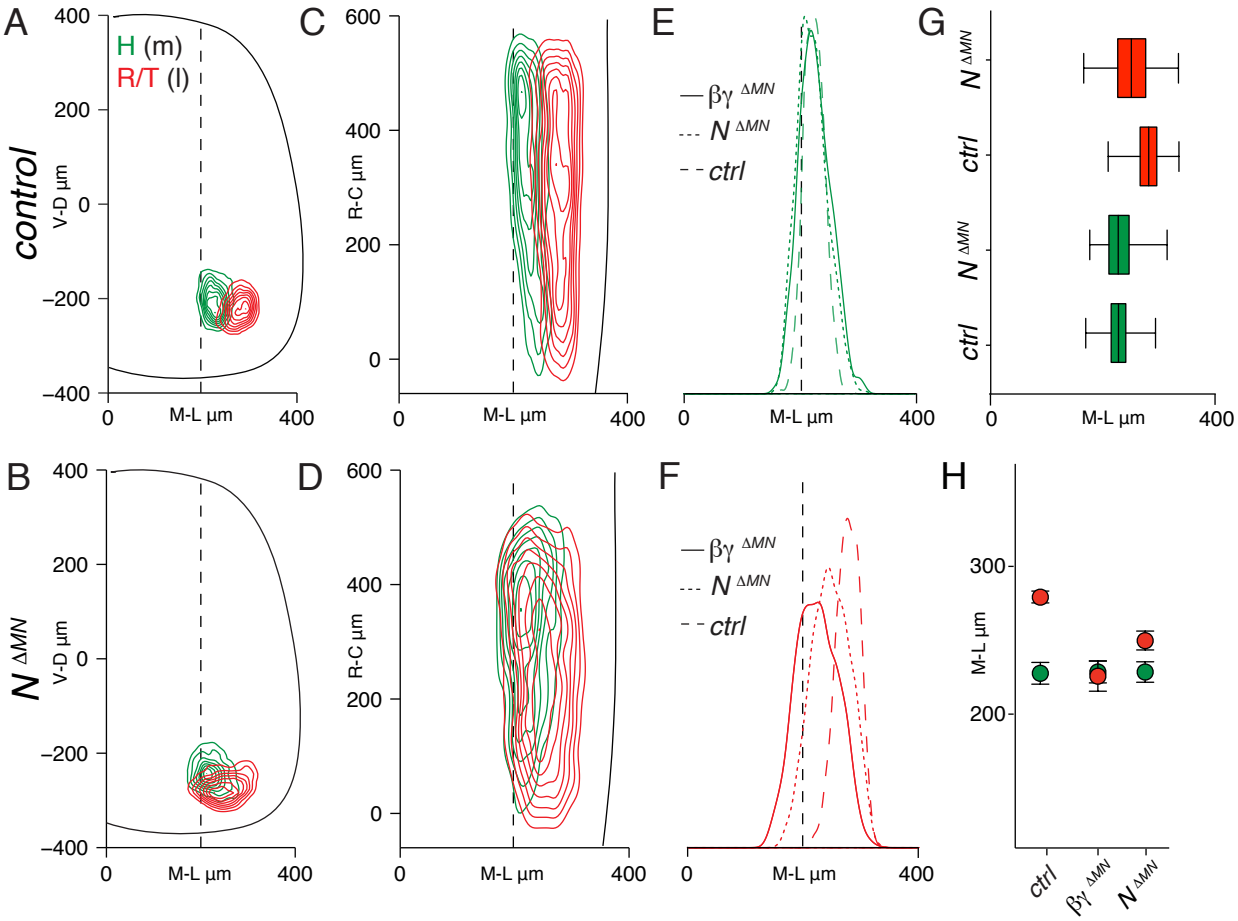

Figure S3. Motor pool organization in e13.5 N-cadherin mutant embryos, related to Figure 4.
(A and B) Transverse contour density analyses of H (green; medial) and R/T (red; lateral) motor pools in *control* and $N^{\Delta MN}$ embryos.
(C and D) Longitudinal contour density analyses of H (green; medial) and R/T (red; lateral) motor pools in *control* and $N^{\Delta MN}$ embryos.
(E) Medio-lateral density analysis of H (green; medial) motor pool in *control*, $N^{\Delta MN}$ and $\beta\gamma^{\Delta MN}$ embryos.
(F) Medio-lateral density analysis of R/T (red/; lateral) motor pool in *control*, $\beta\gamma^{\Delta MN}$ and $N^{\Delta MN}$ embryos.
(G) Box-plots showing medio-lateral distributions of H (green) and R/T (red) neurons in *control* and $N^{\Delta MN}$ embryos.
(H) Average medio-lateral position of H (green; medial) and R/T (red; lateral) motor pools in *control*, $N^{\Delta MN}$ and $\beta\gamma^{\Delta MN}$ embryos (mean ± STDEV; differences significant for R/T neurons $p<0.001$: *control* vs $N^{\Delta MN}$ $p<0.01$; *control* vs $\beta\gamma^{\Delta MN}$ $p<0.001$; $N^{\Delta MN}$ vs $\beta\gamma^{\Delta MN}$ $p<0.05$. One-way ANOVA followed by post-hoc Tukey's HSD test).

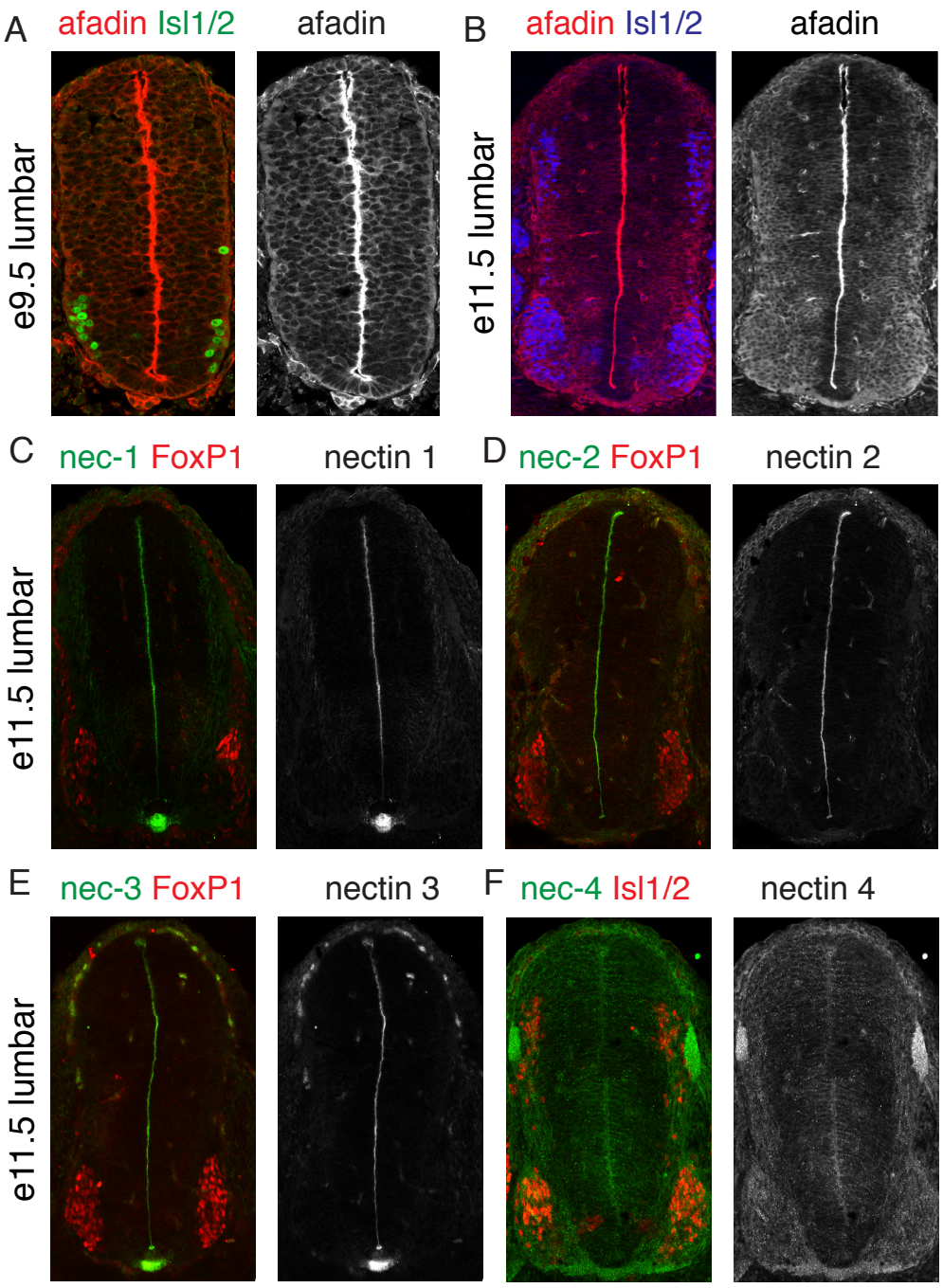

Figure S4. Afadin and nectins expression in the developing spinal cord, related to Figures 5.
(A) Afadin expression at lumbar spinal level of e9.5 wild-type embryos.
(B) Afadin expression at lumbar spinal level of e11.5 wild-type embryos.
(C) Nectin 1 expression at lumbar spinal level of e11.5 wild-type embryos.
(D) Nectin 2 expression at lumbar spinal level of e11.5 wild-type embryos.
(E) Nectin 3 expression at lumbar spinal level of e11.5 wild-type embryos.
(F) Nectin 4 expression at lumbar spinal level of e11.5 wild-type embryos.

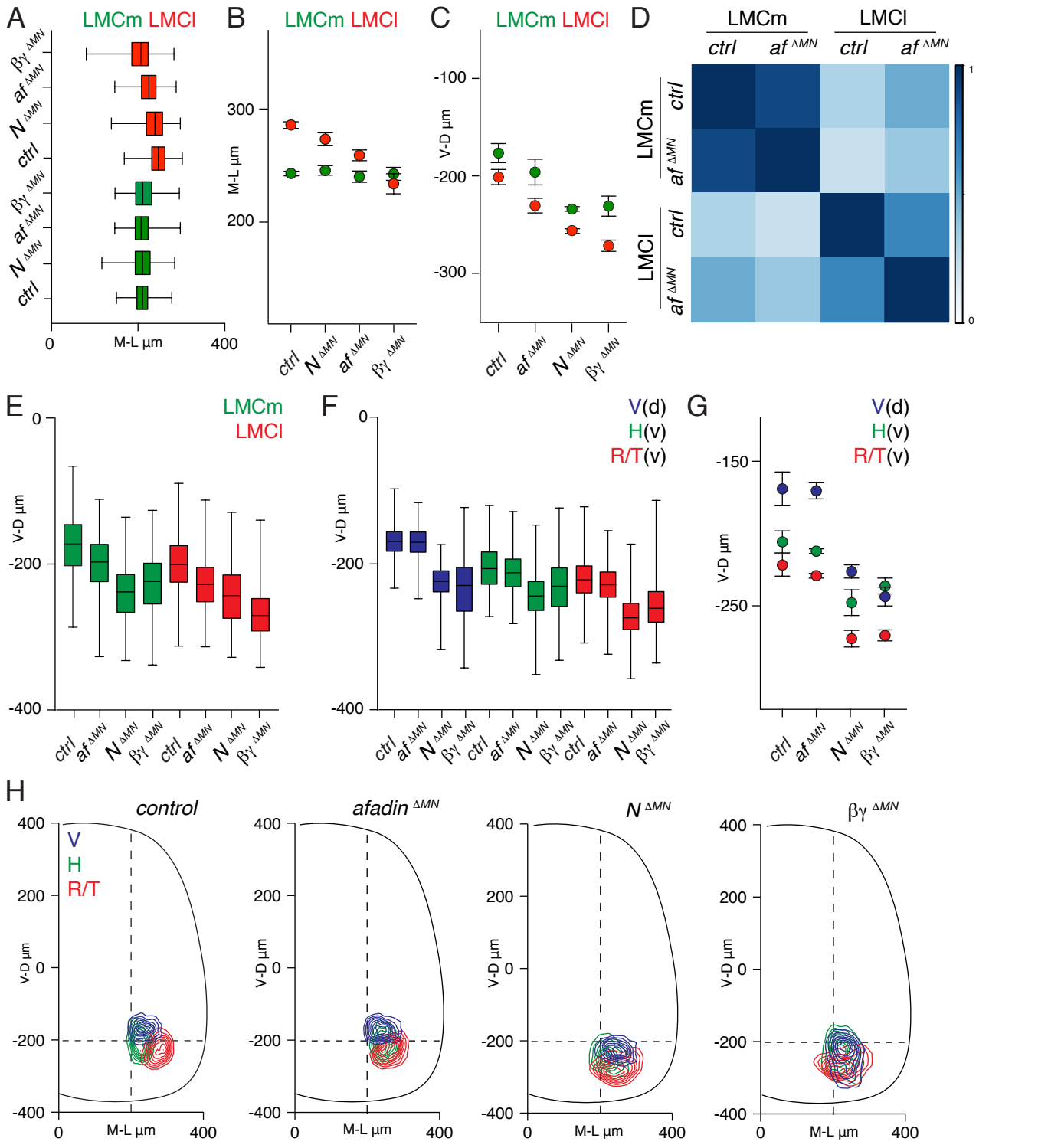

Figure S5. Pool and divisional positional analysis in e13.5 embryos, related to Figure 7.
(A) Box-plots showing medio-lateral distributions of LMCm (green) and LMCl (red) neurons in *control*, $N^{\Delta MN}$, *afadin*$^{\Delta MN}$ and $\beta\gamma^{\Delta MN}$ embryos.(B) Average medio-lateral positions of LMCm (green) and LMCl (red) neurons in *control*, $N^{\Delta MN}$, *afadin*$^{\Delta MN}$ and $\beta\gamma^{\Delta MN}$ embryos (mean ± STDEV; differences significant for LMCl neurons p<0.001: *control* vs *afadin*$^{\Delta MN}$ p<0.01, *control* vs $\beta\gamma^{\Delta MN}$ p<0.001, *afadin*$^{\Delta MN}$ vs $\beta\gamma^{\Delta MN}$ p<0.05, $N^{\Delta MN}$ vs $\beta\gamma^{\Delta MN}$ p<0.001. One-way ANOVA followed by post-hoc Tukey's HSD test). (C) Average dorso-ventral position of LMCm (green) and LMCl (red) neurons in *control*, $N^{\Delta MN}$, *afadin*$^{\Delta MN}$ and $\beta\gamma^{\Delta MN}$ embryos (mean ± STDEV; differences significant for LMCm neurons p<0.001: *control* vs $N^{\Delta MN}$ p<0.001, control vs. $\beta\gamma^{\Delta MN}$ p<0.001, *afadin*$^{\Delta MN}$ vs $\beta\gamma^{\Delta MN}$ p<0.01, *afadin*$^{\Delta MN}$ vs $N^{\Delta MN}$ p<0.01. For LMCl neurons p<0.001: *control* vs *afadin*$^{\Delta MN}$ p<0.05, *control* vs $N^{\Delta MN}$ p<0.001, *control* vs. $\beta\gamma^{\Delta MN}$ p<0.001, *afadin*$^{\Delta MN}$ vs $N^{\Delta MN}$ p<0.05, *afadin*$^{\Delta MN}$ vs $\beta\gamma^{\Delta MN}$ p<0.01. One-way ANOVA followed by post-hoc Tukey's HSD test). (D) Correlation analysis of LMCm and LMCl positional coordinates in *control* and *afadin*$^{\Delta MN}$ embryos. Scale bar indicates correlation values.(E) Box-plots showing dorso-ventral distributions of LMCm (green) and LMCl (red) neurons in *control*, *afadin*$^{\Delta MN}$, $N^{\Delta MN}$ and $\beta\gamma^{\Delta MN}$ embryos. (F) Box-plots showing dorso-ventral distribution of V (blue; dorsal), H (green; ventral) and R/T (red; ventral) motor pools in *control*, *afadin*$^{\Delta MN}$, $N^{\Delta MN}$ and $\beta\gamma^{\Delta MN}$ embryos. (G) Average dorso-ventral position of V (blue; dorsal), H (green; ventral) and R/T (red; ventral) motor pools in *control*, *afadin*$^{\Delta MN}$, $N^{\Delta MN}$ and $\beta\gamma^{\Delta MN}$ embryos (mean ± STDEV; differences significant for V neurons p<0.001: *control* vs $N^{\Delta MN}$ p<0.001, *control* vs. $\beta\gamma^{\Delta MN}$ p<0.001, *afadin*$^{\Delta MN}$ vs $N^{\Delta MN}$ p<0.001, *afadin*$^{\Delta MN}$ vs $\beta\gamma^{\Delta MN}$ p<0.001. For R/T neurons p<0.001: *control* vs $N^{\Delta MN}$ p<0.001, *control* vs. $\beta\gamma^{\Delta MN}$ p<0.001,*afadin*$^{\Delta MN}$ vs $N^{\Delta MN}$ p<0.001, *afadin*$^{\Delta MN}$ vs $\beta\gamma^{\Delta MN}$ p<0.001. For H neurons p<0.001: *control* vs $N^{\Delta MN}$p<0.001, *control* vs. $\beta\gamma^{\Delta MN}$ p<0.01, *afadin*$^{\Delta MN}$ vs $N^{\Delta MN}$ p<0.01, *afadin*$^{\Delta MN}$ vs $\beta\gamma^{\Delta MN}$ p<0.05. One-way ANOVA followed by post-hoc Tukey's HSD test). (H) Transverse contour density analyses of V (blue), H (green) and R/T (red) motor pools in *control*, *afadin*$^{\Delta MN}$, $N^{\Delta MN}$ and $\beta\gamma^{\Delta MN}$ embryos.

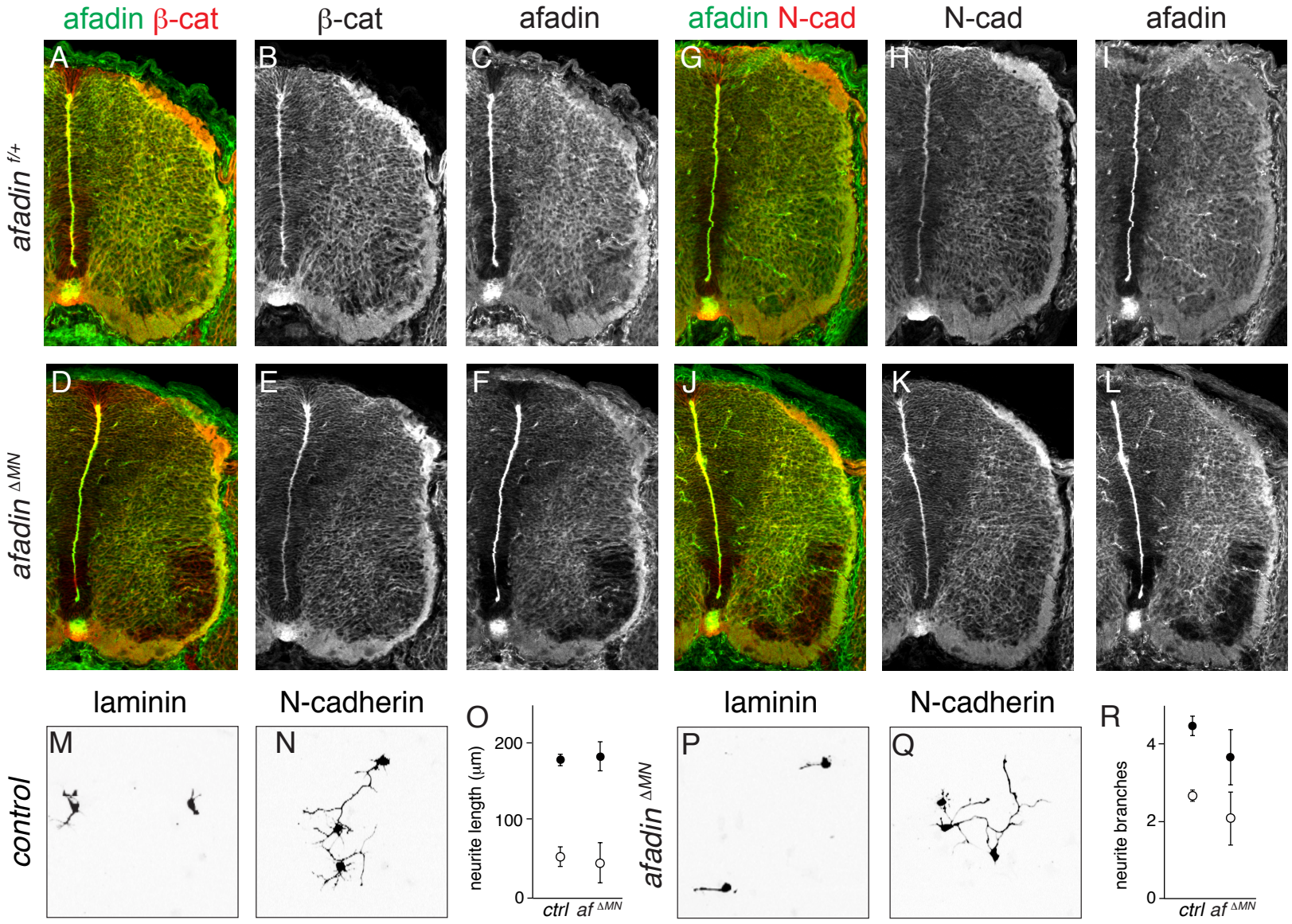

Figure S6. N-cadherin/catenin expression and function in afadin mutant motor neurons, related to Figure 7.
(A-F) Afadin and β-catenin expression in e13.5 *control* and *afadin*$^{\Delta MN}$ embryos.
(G-L) Afadin and N-cadherin expression in e13.5 *control* and *afadin*$^{\Delta MN}$ embryos.
(M-P) Neurite outgrowth of motor neurons, dissociated from *control* (*afadin*$^{fl/+}$*; olig2::Cre*$^{+/-}$; *rosa-lsl-tdTomato*$^{fl/+}$) and *afadin*$^{\Delta MN}$ (*afadin*$^{fl/-}$; *olig2::Cre*$^{+/-}$; *rosa-lsl-tdTomato*$^{fl/+}$) e10.5 embryos and seeded on dishes coated with laminin or N-cadherin. Motor neurons visualized by tdTomato immunoreactivity depicted in black.
(Q and R) Average motor neuron neurite length and branching grown on laminin (○) or N-cadherin (●) for *control* and *afadin*$^{\Delta MN}$ mutant embryos (mean ± STDEV, n=3).